Chapter 10

Post-main sequence evolution through helium burning

After the main-sequence phase, stars are left with a hydrogen-exhausted core surrounded by a still hydrogen-rich envelope. To describe the evolution after the main sequence, it is useful to make a division based on the mass:

low-mass stars are those that develop a degenerate helium core after the main sequence, leading to a relatively long-lived *red giant branch* phase. The ignition of He is unstable and occurs in a so-called *helium flash*. This occurs for masses between $0.8\,M_\odot$ and $\approx 2\,M_\odot$ (this upper limit is sometimes denoted as $M_{\rm HeF}$).

intermediate-mass stars develop a helium core that remains non-degenerate, and they ignite helium in a stable manner. After the central He burning phase they form a carbon-oxygen core that becomes degenerate. Intermediate-mass stars have masses between $M_{\rm HeF}$ and $M_{\rm up} \approx 8\,M_\odot$. Both low-mass and intermediate-mass stars shed their envelopes by a strong stellar wind at the end of their evolution and their remnants are CO white dwarfs.

massive stars have masses larger than $M_{\rm up} \approx 8\,M_\odot$ and ignite carbon in a non-degenerate core. Except for a small mass range ($\approx 8-11\,M_\odot$) these stars also ignite heavier elements in the core until an Fe core is formed which collapses.

In this chapter the evolution between the end of the main sequence and the development of a carbon-oxygen core is discussed. We concentrate on low-mass and intermediate-mass stars, but the principles are equally valid for massive stars. The evolution of massive stars in the H-R diagram is, however, also strongly affected by mass loss and we defer a more detailed discussion of massive stars until Chapter 12.

10.1 The Schönberg-Chandrasekhar limit

During central hydrogen burning on the main sequence, we have seen that stars are in thermal equilibrium ($\tau_{\rm nuc} \gg \tau_{\rm KH}$) with the surface luminosity balanced by the nuclear power generated in the centre. After the main sequence a hydrogen-exhausted core is formed inside which nuclear energy production has ceased. This inert helium core is surrounded by a hydrogen-burning shell and a H-rich envelope. For such an inert core to be in thermal equilibrium requires a zero net energy flow, $l(m) = \int_m \epsilon_{\rm nuc}\,{\rm d}m = 0$ and hence ${\rm d}T/{\rm d}r \propto l = 0$. This implies that the core must be *isothermal* to remain in TE. Such a stable situation is possible only under certain circumstances.

A star composed of ideal gas at constant temperature corresponds to a polytrope with $\gamma = 1$, i.e. with $n \to \infty$. Such a polytrope would have infinite radius (Chapter 4) or, if its radius were finite, would have infinitely high central density, both of which are unphysical. In other words, *completely isothermal stars made of ideal gas cannot exist*. The reason is that the pressure gradient needed to support such a star against its own gravity is produced only by the density gradient, $\mathrm{d}P/\mathrm{d}r = (\mathcal{R}T/\mu)\,\mathrm{d}\rho/\mathrm{d}r$, with no help from a temperature gradient. Thus hydrostatic equilibrium in an isothermal star would require a very large density gradient.

It turns out, however, that if only the core of the star is isothermal, and the mass M_c of this isothermal core is only a small fraction of the total mass of the star, then a stable configuration is possible. If the core mass exceeds this limit, then the pressure within the isothermal core cannot sustain the weight of the overlying envelope. This was first discovered by Schönberg and Chandrasekhar in 1942, who computed the maximum core mass fraction $q_\mathrm{c} = M_\mathrm{c}/M$ to be

$$\frac{M_\mathrm{c}}{M} < q_\mathrm{SC} = 0.37\left(\frac{\mu_\mathrm{env}}{\mu_\mathrm{c}}\right)^2 \approx 0.10 \tag{10.1}$$

where μ_c and μ_env are the mean molecular weight in the core and in the envelope respectively. This limit is known as the *Schönberg-Chandrasekhar limit*. The typical value $q_\mathrm{SC} \approx 0.10$ is appropriate for a helium core with $\mu_\mathrm{c} = 1.3$ and a H-rich envelope. (A simple, qualitative derivation of eq. 10.1 can be found in Maeder Section 25.5.1.)

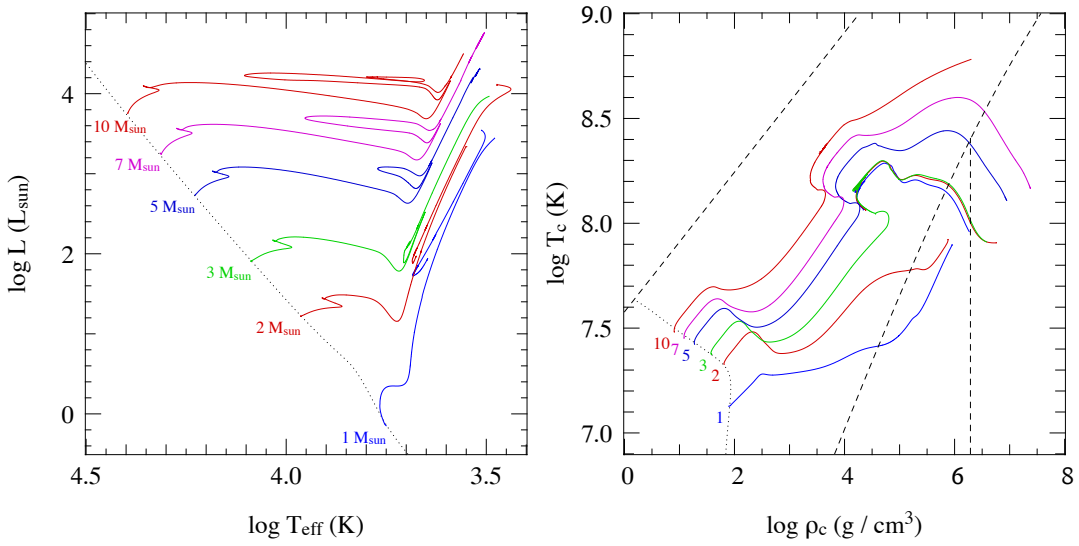

Figure 10.1. Evolution tracks for stars of quasi-solar composition ($X = 0.7$, $Z = 0.02$) and masses of 1, 2, 3, 5, 7 and 10 $M_\odot$ in the H-R diagram (left panel) and in the central temperature versus density plane (right panel). Dotted lines in both diagrams show the ZAMS, while the dashed lines in the right-hand diagram show the borderlines between equation-of-state regions (as in Fig. 3.4). The 1 $M_\odot$ model is characteristic of low-mass stars: the central core becomes degenerate soon after leaving the main sequence and helium is ignited in an unstable flash at the top of the red giant branch. When the degeneracy is eventually lifted, He burning becomes stable and the star moves to the *zero-age horizontal branch* in the HRD, at $\log L \approx 1.8$. The 2 $M_\odot$ model is a borderline case that just undergoes a He flash. The He flash itself is not computed in these models, hence a gap appears in the tracks. The 5 $M_\odot$ model is representative of intermediate-mass stars, undergoing quiet He ignition and He burning in a loop in the HRD. The appearance of the 7 and 10 $M_\odot$ models in the HRD is qualitatively similar. However, at the end of its evolution the 10 $M_\odot$ star undergoes carbon burning in the centre, while the cores of lower-mass stars become strongly degenerate. (Compare to Fig. 8.4.)

Stars that leave the main sequence with a helium core mass below the Schönberg-Chandrasekhar limit can therefore remain in complete equilibrium (HE and TE) during hydrogen-shell burning. This is the case for stars with masses up to about $8\,M_\odot$, if convective overshooting is neglected. Overshooting increases the core mass at the end of central H-burning, and therefore the upper mass limit for stars remaining in TE after the main sequence decreases to about $2\,M_\odot$ in calculations that include moderate overshooting.

When the mass of the H-exhausted core exceeds the Schönberg-Chandrasekhar limit – either immediately after the main sequence in relatively massive stars, or in lower-mass stars after a period of H-shell burning during which the helium core mass increases steadily – thermal equilibrium is no longer possible. The helium core then contracts and builds up a temperature gradient. This temperature gradient adds to the pressure gradient that is needed to balance gravity and keep the star in HE. However, the temperature gradient also causes an outward heat flow from the core, such that it keeps contracting and heating up in the process (by virtue of the virial theorem). This contraction occurs on the thermal (Kelvin-Helmholtz) timescale in a quasi-static way, always maintaining a state very close to HE.

Low-mass stars ($M \lesssim 2\,M_\odot$) have another way of maintaining both HE and TE during hydrogen-shell burning. In such stars the helium core is relatively dense and cool and electron degeneracy can become important in the core after the main sequence. Degeneracy pressure is independent of temperature and can support the weight of the envelope even in a relatively massive core, as long as the degenerate core mass does not exceed the Chandrasekhar mass.[1] In that case the Schönberg-Chandrasekhar limit no longer applies. Inside such degenerate helium cores efficient energy transport by *electron conduction* (Sec. 5.2.4) can keep the core almost isothermal.

Effects of core contraction: the 'mirror principle'

The following principle appears to be generally valid, and provides a way of interpreting the results of detailed numerical calculations:

Whenever a star has an *active shell-burning source*, the burning shell acts as a *mirror* between the core and the envelope:

core contraction $\Rightarrow$ envelope expansion
core expansion $\Rightarrow$ envelope contraction

This 'mirror principle' can be understood by the following argument. To maintain thermal equilibrium, the burning shell must remain at approximately constant temperature due to the thermostatic action of nuclear burning. Contraction of the burning shell would entail heating, so the burning shell must also remain at roughly constant radius. As the core contracts, $\rho_{\rm shell}$ must therefore decrease and hence also the pressure in the burning shell must decrease. Therefore the pressure $P_{\rm env}$ of the overlying envelope must decrease, so the layers above the shell must expand (an example of this behaviour can be seen in Fig. 10.4, to be discussed in the next section).

10.2 The hydrogen-shell burning phase

In this section we discuss in some detail the evolution of stars during hydrogen-shell burning, until the onset of helium burning. Based on the above section, qualitative differences are to be expected between low-mass stars ($M \lesssim 2\,M_\odot$) on the one hand and intermediate- and high-mass stars ($M \gtrsim$

[1] Note the very different physical meanings of the *Chandrasekhar mass* and the *Schönberg-Chandrasekhar limit*!

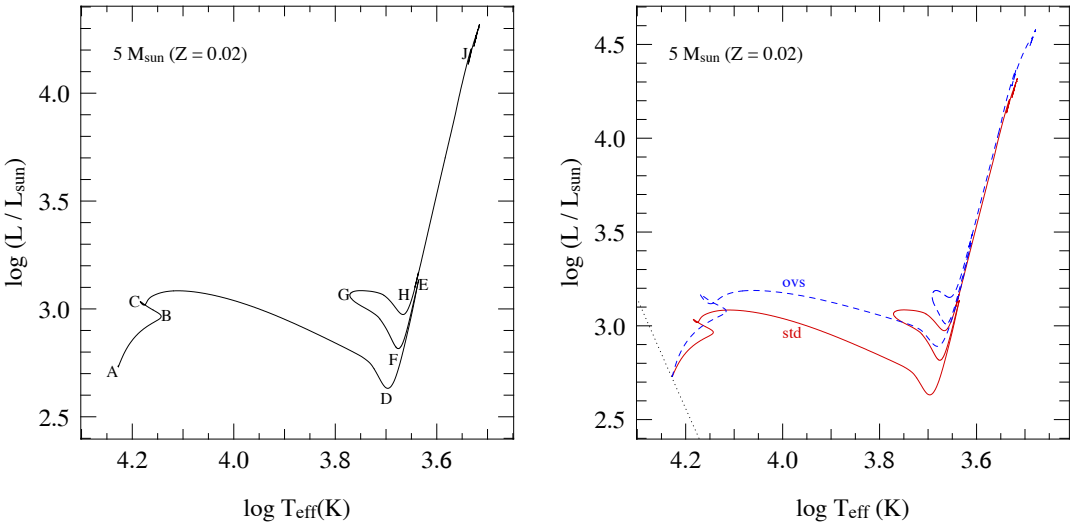

Figure 10.2. Evolution track in the Hertzsprung-Russell diagram of a $5\,M_\odot$ star of initial composition $X = 0.7$, $Z = 0.02$. See text for details. The evolution track in the left panel was computed without convective overshooting. The right panel shows a comparison between this track and the evolution of the same star computed with moderate overshooting ($\alpha_{\rm ov} = l_{\rm ov}/H_P \approx 0.25$; dashed line), illustrating some of the effects discussed in Sec. 9.3.4.

$2\,M_\odot$) on the other hand. Therefore we discuss these two cases separately, starting with the evolution of higher-mass stars because it is relatively simple compared to low-mass stars. We use two detailed stellar evolution sequences, for stars of $5\,M_\odot$ and $1\,M_\odot$ respectively, as examples for the general evolutionary behaviour of stars in these two mass ranges.

10.2.1 Hydrogen-shell burning in intermediate-mass and massive stars

Fig. 10.2 shows the evolution track of a $5\,M_\odot$ star of quasi-solar composition ($X = 0.7, Z = 0.02$) in the H-R diagram, and Fig. 10.3 shows some of the interior details of the evolution of this star as a function of time from the end of central hydrogen burning. Point B in both figures corresponds to the start of the overall contraction phase near the end of the main sequence (when the central H mass fraction $X_c \approx 0.03$) and point C corresponds to the exhaustion of hydrogen in the centre and the disappearance of the convective core. The hatched regions in the 'Kippenhahn diagram' (lower panel of Fig. 10.3) show the rapid transition at point C from hydrogen burning in the centre to hydrogen burning in a shell.

The H-exhausted core initially has a mass of about $0.4\,M_\odot$ which is below the Schönberg-Chandrasekhar limit, so the star initially remains in TE and the first portion of the hydrogen-shell burning phase (C–D) is relatively slow, lasting about 2×10^6 yr. The temperature and density gradients between core and envelope are still shallow, so that the burning shell initially occupies a rather large region in mass. This phase is therefore referred to as *thick shell burning*. The helium core gradually grows in mass until it exceeds the S-C limit and the contraction of the core speeds up. The envelope expands at the same time, exemplifying the 'mirror principle' discussed above. This becomes more clear in Fig. 10.4 which shows the radial variations of several mass shells inside the star. After point C the layers below the burning shell contract while the layers above expand, at an accelerating rate towards the end of phase C–D. As a result the temperature and density gradients between core and

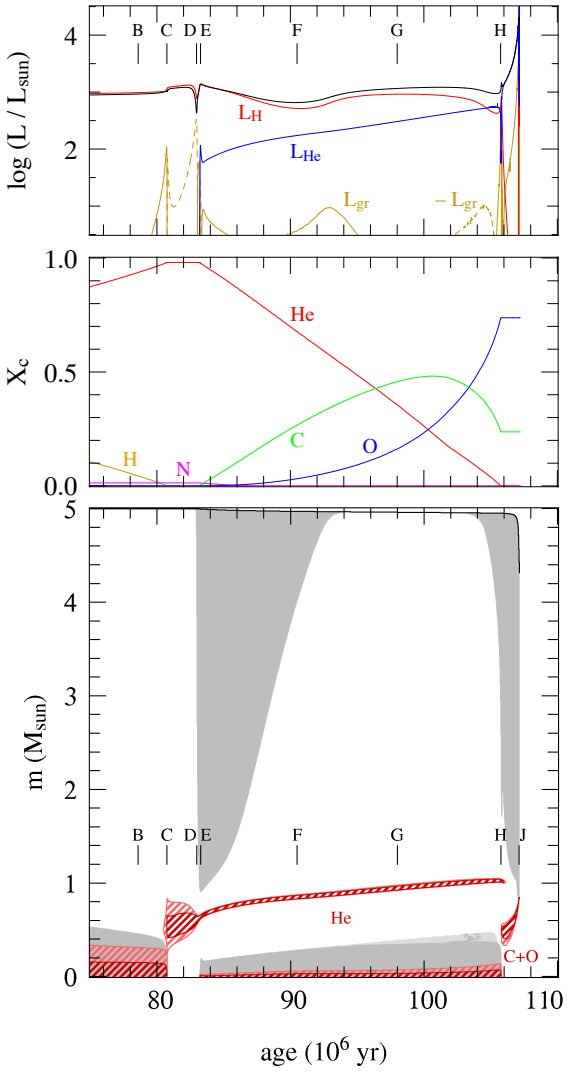

Figure 10.3. Internal evolution of a 5 $M_\odot$ star of initial composition $X = 0.7, Z = 0.02$. The panels show various internal quantities as a function of time, from top to bottom:

(a) Contributions to the luminosity from hydrogen burning (red line), helium burning (blue) and gravitational energy release (orange; dashed parts show net *absorption* of gravitational energy). The black line is the surface luminosity.

(b) Central mass fractions of various elements (^{1}H, ^{4}He, ^{12}C, ^{14}N and ^{16}O) as indicated.

(c) Internal structure as a function of mass coordinate m, known as a 'Kippenhahn diagram'. A vertical line through the graph corresponds to a model at a particular time. Gray areas are convective, lighter-gray areas are semi-convective. The red hatched regions show areas of nuclear energy generation, where $\epsilon_{\rm nuc} > 10\,L/M$ (dark red) and $\epsilon_{\rm nuc} > 2\,L/M$ (light red). The letters B…J indicate the corresponding points in the evolution track in the H-R diagram, plotted in Fig. 10.2. See text for details.

envelope increase, and the burning shell occupies less and less mass (Fig. 10.3c). The latter portion of hydrogen-shell burning is therefore referred to as *thin shell burning*. Most of the time between C and D is spent in the thick shell burning phase at relatively small radii and $\log T_{\rm eff} > 4.05$. The phase of expansion from $\log T_{\rm eff} \approx 4.05$ to point D at $\log T_{\rm eff} \approx 3.7$ occurs on the Kelvin-Helmholtz timescale and takes only a few times 10^5 yrs. A substantial fraction of the energy generated by shell burning is absorbed by the expanding envelope (dashed yellow line in Fig. 10.3a), resulting in a decrease of the surface luminosity between C and D.

The rapid evolution on a thermal timescale across the H-R diagram from the end of the main sequence to $T_{\rm eff} \approx 5000$ K is characteristic of all intermediate-mass stars. The probability of detecting stars during this short-lived phase is very small, resulting in a gap in the distribution of stars in the H-R diagram known as the *Hertzsprung gap*.

As point D is approached the envelope temperature decreases and the opacity in the envelope rises, impeding radiative energy transport. The envelope grows increasingly unstable to convection, starting from the surface, until at D a large fraction of the envelope mass has become convective. During

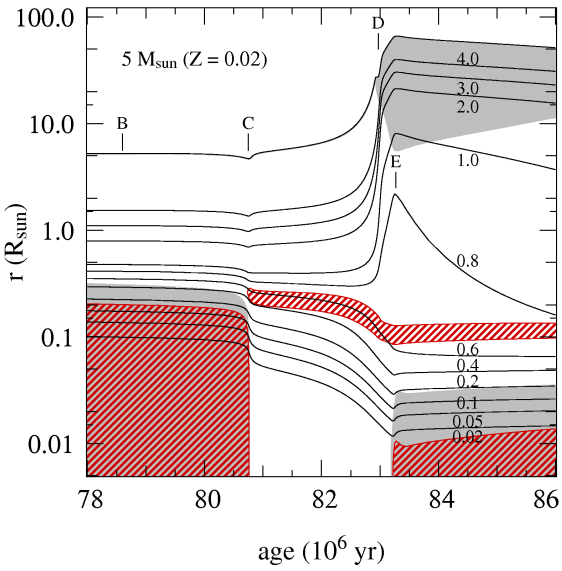

Figure 10.4. Radial variation of various mass shells (solid lines) in the 5 $M_\odot$ ($Z = 0.02$) star of Fig. 10.3, during the early post-main sequence evolution. Each line is labelled with its mass coordinate m in units of $M_\odot$; the top-most curve indicates the total radius R. Gray areas indicate convection and red cross-hatched areas have intense nuclear burning ($\epsilon_{\rm nuc} > 10\,L/M$). Letters B…E correspond to those in Fig. 10.3.

phase D–E the star is a red giant with a deep convective envelope. The star is then located close to the Hayashi line in the H-R diagram, and while it continues to expand in response to core contraction, the luminosity increases as the effective temperature remains at the approximately constant value corresponding to the Hayashi line. The expansion of the star between D and E still occurs on the thermal timescale, so the H-shell burning phase of intermediate-mass stars on the red-giant branch is very short-lived.

At its deepest extent at point E, the base of the convective envelope is located at mass coordinate $m = 0.9\,M_\odot$ which is below the maximum extent of the former convective core during central H-burning (about 1.25 $M_\odot$ at the start of the main sequence). Hence material that was formerly inside the convective core, and has therefore been processed by hydrogen burning and the CNO-cycle, is mixed throughout the envelope and appears at the surface. This process is called *dredge-up* and occurs about halfway between D and E in Fig. 10.2. Dredge-up on the red giant branch also occurs in low-mass stars and we defer its discussion to Sec. 10.2.3.

The helium cores of intermediate-mass stars remain non-degenerate during the entire H-shell burning phase C–E, as can be seen in Fig. 10.1. These stars develop helium cores with masses larger than 0.3 $M_\odot$, the minimum mass for helium fusion discussed in Ch. 8. In the 5 $M_\odot$ star at point E the helium core mass is 0.6 $M_\odot$ when a central temperature of 10^8 K is reached and helium is ignited in the core. The ignition of helium halts further core contraction and envelope expansion and therefore corresponds to a local maximum in luminosity and radius. Evolution through helium burning will be discussed in Sec. 10.3.1.

10.2.2 Hydrogen-shell burning in low-mass stars

Compared to intermediate-mass stars, low-mass stars (with $M \lesssim 2\,M_\odot$) have small or no convective cores during central hydrogen burning, and when they leave the main sequence their cores are relatively dense and already close to becoming degenerate (see Fig. 10.1). In stars with $M \lesssim 1.1\,M_\odot$ the transition from central to shell hydrogen burning is gradual and initially $M_{\rm c}/M < 0.1$ so the star can remain in thermal equilibrium with an isothermal helium core. By the time the helium core has grown to $\approx 0.1M$, its density is large enough that electron degeneracy dominates the pressure and the

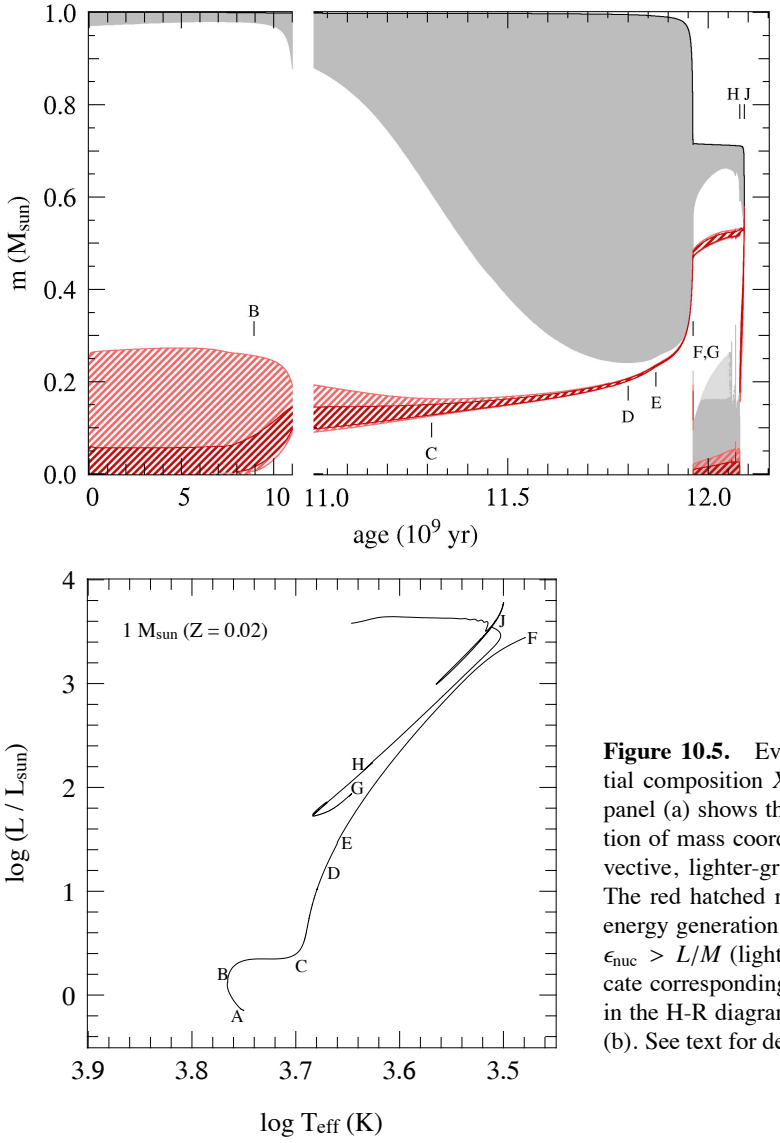

Figure 10.5. Evolution of a $1\,M_\odot$ star of initial composition $X = 0.7$, $Z = 0.02$. The top panel (a) shows the internal structure as a function of mass coordinate m. Gray areas are convective, lighter-gray areas are semi-convective. The red hatched regions show areas of nuclear energy generation: $\epsilon_{\rm nuc} > 5\,L/M$ (dark red) and $\epsilon_{\rm nuc} > L/M$ (light red). The letters A…J indicate corresponding points in the evolution track in the H-R diagram, plotted in the bottom panel (b). See text for details.

Schönberg-Chandrasekhar limit has become irrelevant. Therefore low-mass stars can remain in HE and TE throughout hydrogen-shell burning and there is no Hertzsprung gap in the H-R diagram.

This can be seen in Fig. 10.5 which shows the internal evolution of a $1\,M_\odot$ star with quasi-solar composition in a Kippenhahn diagram and the corresponding evolution track in the H-R diagram. Hydrogen is practically exhausted in the centre at point B ($X_c = 10^{-3}$) after 9 Gyr, after which nuclear energy generation gradually moves out to a thick shell surrounding the isothermal helium core. Between B and C the core slowly grows in mass and contracts, while the envelope expands in response and the burning shell gradually becomes thinner in mass. By point C the helium core has become degenerate. At the same time the envelope has cooled and become largely convective, and the star finds itself at the base of the *red giant branch* (RGB), close to the Hayashi line. The star remains in thermal equilibrium throughout this evolution and phase B–C lasts about 2 Gyr for this $1\,M_\odot$ star. This long-lived phase corresponds to the well-populated *subgiant branch* in the H-R diagrams of old

star clusters.

Stars with masses in the mass range $1.1 - 1.5\,M_\odot$ show a very similar behaviour after the main sequence, the only difference being the small convective core they develop during core H-burning. This leads to a 'hook' in the evolution track at central H exhaustion (see Sec. 9.3). The subsequent evolution during H-shell burning is similar, the core remaining in TE until it becomes degenerate on the RGB and a correspondingly slow evolution across the subgiant branch. Stars with $1.5 \lesssim M/M_\odot \lesssim 2$ do exhibit a small Hertzsprung gap as they reach the Schönberg-Chandrasekhar limit before their cores become degenerate. After a period of slow, thick shell burning on the subgiant branch they undergo a phase of rapid, thermal-timescale expansion until they reach the giant branch. In this case the gap in $T_{\rm eff}$ to be bridged is narrow because the main sequence is already relatively close in effective temperature to the Hayashi line.

Regardless of these differences between stars of different mass during the early shell-H burning phase, all stars with $M \lesssim 2\,M_\odot$ have in common that their helium cores become degenerate before the central temperature is high enough for helium ignition, and they settle into TE on the red giant branch.

10.2.3 The red giant branch in low-mass stars

The evolution of low-mass stars along the red giant branch is very similar and almost independent of the mass of the star. The reason for this similarity is that by the time the helium core has become degenerate, a very strong density contrast has developed between the core and the envelope. The envelope is so extended that it exerts very little weight on the compact core, while there is a very large pressure gradient between core and envelope. The pressure at the bottom of the envelope (see eq. 9.14) is very small compared to the pressure at the edge of the core and in the hydrogen-burning shell separating core and envelope. Therefore the stellar structure depends almost entirely on the properties of the helium core. Since the core is degenerate, its structure is independent of its thermal properties (temperature) and only depends on its mass. Therefore the structure of a low-mass red giant is essentially a function of its *core mass*.

As a result there is a very tight relation between the helium core mass and the luminosity of a red giant, which is entirely due to the hydrogen shell-burning source. This *core-mass luminosity* relation is very steep for small core masses, $M_{\rm c} \lesssim 0.5\,M_\odot$ and can be approximately described by a power law

$$L \approx 2.3 \times 10^5 L_\odot \left(\frac{M_{\rm c}}{M_\odot}\right)^6 \tag{10.2}$$

Note that the luminosity of a low-mass red giant is independent of its total mass. Therefore the evolution of all stars with $M \lesssim 2\,M_\odot$ converges after the core becomes degenerate, which occurs when $M_{\rm c} \approx 0.1M$, i.e. later for larger M. From this point on also the central density and temperature start following almost the same evolution track (e.g. see Fig. 10.1b).

In the H-R diagram the star is located along the Hayashi line appropriate for its mass M. Higher-mass red giants therefore have slightly higher $T_{\rm eff}$ at the same luminosity.[2] Note that the location of the Hayashi line also depends on the *metallicity* of the star, since the effective temperature of a completely convective star is determined by the H^- opacity in the photosphere (Sec. 9.1.1). Because the H^- opacity increases with metallicity (Sec. 5.3), more metal-rich red giants of the same mass and luminosity are located at lower $T_{\rm eff}$. This provides a means of deriving the metallicity of a globular cluster from the location of its RGB stars in the H-R diagram.

[2]This means there is also a *core-mass radius* relation, but it is less tight than the $M_{\rm c}$-L relation and depends slightly on the total mass.

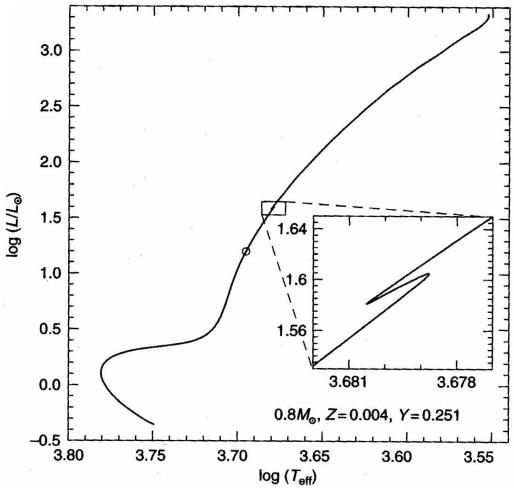

Figure 10.6. Evolution track of a $0.8\,M_\odot$ star of rather low metallicity, $Z = 0.004$. The inset shows the temporary decrease of luminosity when the H-burning shell crosses the hydrogen discontinuity left by the first dredge-up (corresponding to point E in Fig. 10.5). The open circle indicates where first dredge-up occurs. Figure from Salaris & Cassisi.

As the H-burning shell adds mass to the degenerate helium core, the core slowly contracts and the radius and luminosity increase. The higher luminosity means the H-shell must burn at a higher rate, leading to faster core-mass growth. The evolution along the RGB thus speeds up as the luminosity increases (see Fig. 10.5). The density contrast between core and envelope increases and the mass within the burning shell decreases, to $\approx 0.001\,M_\odot$ near the tip of the RGB. Since less mass is contained in the burning shell while the luminosity increases, the energy generation rate per unit mass $\epsilon_{\rm nuc}$ increases strongly, which means the temperature within the burning shell also increases. With it, the temperature in the degenerate helium core increases. When the tip of the RGB is reached (at point F in Fig. 10.5) at $L \approx 2000\,L_\odot$ and a core mass of $\approx 0.45\,M_\odot$, the temperature in the degenerate core has reached a value close to 10^8 K and helium is ignited. This is an unstable process due to the strong degeneracy, and leads to a thermonuclear runaway known as the *helium flash* (see Sec. 10.3.2).

First dredge-up and the luminosity bump

When the convective envelope reaches its deepest extent at point D in Fig. 10.5, it has penetrated into layers that were processed by H-burning during the main sequence, and have been partly processed by the CN-cycle. Up to point D the surface He abundance increases and the H abundance decreases, but more noticeably the C/N ratio decreases by a large factor. This is called the *first dredge-up* phase (later dredge-ups occur after He burning).

Some time later, at point E in Fig. 10.5 the H-burning shell has eaten its way out to the discontinuity left by the convective envelope at its deepest extent. The shell suddenly finds itself in an environment with a higher H abundance (and a lower mean molecular weight). As a consequence it starts burning at a slightly lower rate, leading to a slight decrease in luminosity (see Fig. 10.6). The resulting loop (the star crosses this luminosity range three times) results in a larger number of stars in this luminosity range in a stellar population. This 'bump' in the luminosity function has been observed in many old star clusters.

Mass loss on the red giant branch

Another process that becomes important in low-mass red giants is *mass loss*. As the stellar luminosity and radius increase as a star evolves along the giant branch, the envelope becomes loosely bound and it is relatively easy for the large photon flux to remove mass from the stellar surface. The process

driving mass loss in red giants is not well understood. When calculating the effect of mass loss in evolution models an empirical formula due to Reimers is often used:

$$\dot{M} = -4 \times 10^{-13}\, \eta\, \frac{L}{L_\odot}\, \frac{R}{R_\odot}\, \frac{M_\odot}{M}\, M_\odot/\mathrm{yr} \tag{10.3}$$

where η is a parameter of order unity. Note that the Reimers formula implies that a fixed fraction of the stellar luminosity is used to lift the wind material out of the gravitational potential well. However, the relation is based on observations of only a handful of stars with well-determined stellar parameters.

A value of $\eta \sim 0.25 - 0.5$ is often used because it gives the right amount of mass loss on the RGB to explain the morphology in the H-R diagram of stars in the subsequent helium-burning phase, on the *horizontal branch*. The 1 $M_\odot$ star of our example loses about 0.3 $M_\odot$ of its envelope mass by the time it reaches the tip of the giant branch.

10.3 The helium burning phase

As the temperature in the helium core approaches 10^8 K, the 3α reaction starts to produce energy at a significant rate. This is the onset of the *helium burning* phase of evolution. Unlike for hydrogen burning, the reactions involved in helium burning (see Sect. 6.4.2) are the same for all stellar masses. However, the conditions in the core at the ignition of helium are very different in low-mass stars (which have degenerate cores) from stars of higher mass (with non-degenerate cores). Therefore these cases will be discussed separately.

10.3.1 Helium burning in intermediate-mass stars

We again take the 5 $M_\odot$ star depicted in Figs. 10.2–10.3 as a typical example of an intermediate-mass star. The ignition of helium takes place at point E in these figures. Since the core is non-degenerate at this point ($\rho_c \approx 10^4$ g/cm^3, Fig. 10.1), nuclear burning is thermally stable and helium ignition proceeds quietly. Owing to the high temperature sensitivity of the He-burning reactions, energy production is highly concentrated towards the centre which gives rise to a convective core. The mass of the convective core is 0.2 $M_\odot$ initially and grows with time (unlike was the case for hydrogen burning).

Initially, the dominant reaction is the 3α reaction which converts ^{4}He into ^{12}C inside the convective core. As the ^{12}C abundance builds up, the $^{12}\mathrm{C}+\alpha$ reaction gradually takes over, so that ^{16}O is also produced at a rate that increases with time (see Fig. 10.3b and compare to Fig. 6.6). When the central He abundance $X_\mathrm{He} < 0.2$ the mass fraction of ^{12}C starts decreasing as a result of the diminishing 3α rate (which is proportional to X_He^3). The final $^{12}\mathrm{C}/^{16}\mathrm{O}$ ratio is about 0.3, decreasing somewhat with stellar mass. This is related to the fact that in more massive stars the central temperature during He burning is larger. Note that the final $^{12}\mathrm{C}/^{16}\mathrm{O}$ ratio depends on the uncertain rate of the $^{12}\mathrm{C}(\alpha,\gamma)$ reaction, and the values given here are for the rate that is currently thought to be most likely.

The duration of the central helium burning phase in our 5 $M_\odot$ star (E–H) is about 22 Myr, i.e. approximately $0.27 \times \tau_\mathrm{MS}$. This seems surprisingly long given that the energy gain per gram of He burning is only 10 % of that of H burning, while the luminosity of the star is (on average) somewhat larger than during the main sequence. The reason can be discerned from Fig. 10.3a: most of the luminosity during helium burning still comes from the H-burning shell surrounding the core, although the luminosity contribution of He burning (L_He) increases with time and becomes comparable towards the end of this phase.

We can understand the behaviour of L_He by considering that the properties of the helium core essentially depend only on the core mass M_c and are hardly affected by the surrounding envelope. Because the envelope is very extended the pressure it exerts on the core (eq. 9.14) is negligible compared

to the pressure inside the dense helium core. In fact $L_{\rm He}$ is a steep function of $M_{\rm c}$, analogous to the main-sequence M-L relation – indeed, if the envelope were stripped away, the bare helium core would lie on a *helium main sequence*. The mass-luminosity relation for such helium main-sequence stars can be approximately described by the homology relation (7.32) if the appropriate value of μ is used. As a result of H-shell burning, $M_{\rm c}$ grows with time during the He-burning phase and $L_{\rm He}$ increases accordingly. Another consequence is that in models computed with convective overshooting $L_{\rm He}$ is larger on account of the larger core mass left after the main sequence (see Sect. 9.3.4). Therefore the duration of the He burning phase (i.e. the appropriate nuclear timescale, $\tau_{\rm nuc} \propto M_{\rm c}/L_{\rm He}$) is *shorter* in models with overshooting. A 5 $M_\odot$ star of the same composition computed with overshooting has a main-sequence lifetime $\tau_{\rm MS} = 100$ Myr and a helium-burning lifetime of 16 Myr.

During helium burning intermediate-mass stars describe a loop in the H-R diagram (E–H in Fig. 10.2). After He ignition at the tip of the giant branch, the envelope contracts (on the nuclear timescale for helium burning) and the stellar radius decreases. Initially the luminosity also decreases while the envelope is mostly convective (E–F) and the star is forced to move along its Hayashi line. When most of the envelope has become radiative at point F, the star leaves the red giant branch and the effective temperature increases. This is the start of a so-called *blue loop*, the hottest point of which is reached at G when $X_{\rm He} \approx 0.3$. This also corresponds to a minimum in the stellar radius, after which the envelope starts expanding and the star again approaches the giant branch when $X_{\rm He} \approx 0.05$. By the end of core helium burning (H) the star is back on the Hayashi line, very close to its starting point (E). If we consider stars of different masses, the blue extension of the loops in the HRD increases (the loops extend to larger $T_{\rm eff}$ values) for increasing mass, up to $M \approx 12\,M_\odot$. (The behaviour of stars of larger masses can be more complicated, one of the reasons being strong mass loss, and we defer a discussion of this until Chapter 12.) On the other hand, for $M \lesssim 4\,M_\odot$ the loops always stay close to the red giant branch and do not become 'blue'.

The occurrence of blue loops is another example of a well-established result of detailed stellar evolution calculations, that is difficult to explain in terms of basic physics. The detailed models indicate that the occurrence and extension of blue loops depends quite sensitively on a number of factors: the chemical composition (mainly Z), the mass of the helium core relative to the envelope, and the shape of the hydrogen abundance profile above the core. It therefore also depends on whether convective overshooting was assumed to take place during the main sequence: this produces a larger core mass, which in turn has the effect of decreasing the blue-ward extension of the loops while increasing their luminosity.

The blue loops are important because they correspond to a slow, nuclear timescale phase of evolution. One therefore expects the corresponding region of the H-R diagram to be well populated. More precisely, since intermediate-mass stars spend part of their He-burning phase as red giants and part of it in a blue loop, one expects such stars to fill a wedge-shaped region in the HRD. Indeed one finds many stars in the corresponding region, both in the solar neighbourhood (Fig. 1.1, although this is dominated by *low-mass* stars) and in open clusters with ages less than ~ 1 Gyr. The dependence of the loops on overshooting also makes observational tests of overshooting using He-burning stars possible. Another significant aspect of blue loops is that they are necessary for explaining Cepheid variables (see Sect. 10.4), which are important extragalactic distance indicators.

10.3.2 Helium burning in low-mass stars

In low-mass stars (with $M \lesssim 2\,M_\odot$) the helium burning phase differs from more massive stars in two important aspects: (1) helium ignition occurs under degenerate conditions, giving rise to a *helium flash*, and (2) all low-mass stars start helium burning with essentially the same core mass $M_{\rm c} \approx 0.45\,M_\odot$ (Sect. 10.2.3). The luminosity of low-mass He-burning stars is therefore almost independent

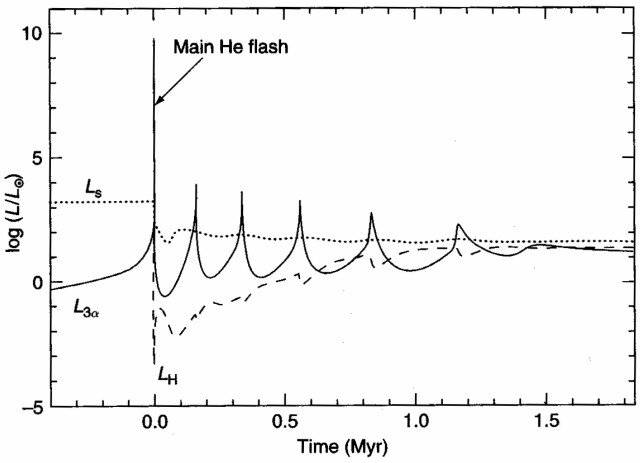

Figure 10.7. The helium flash. Evolution with time of the surface luminosity (L_s), the He-burning luminosity ($L_{3\alpha}$) and the H-burning luminosity ($L_{\rm H}$) during the onset of He burning at the tip of the RGB in a low-mass star. Time $t = 0$ corresponds to the start of the main helium flash. Figure from Salaris & Cassisi.

of their mass, giving rise to a *horizontal branch* in the HRD.

The helium flash

We again take a star of 1 $M_\odot$ as a typical example of all low-mass stars. Helium ignition occurs when $T_c \approx 10^8$ K and $\rho_c \approx 10^6$ g/cm^3, so the helium core is strongly degenerate (see Fig. 10.1). We have seen in Sect. 7.5.2 that helium burning under these conditions is thermally unstable: the energy generated by the 3α reaction causes a temperature increase, rather than a decrease, and helium ignition thus initiates a *thermonuclear runaway*. The reason is that the degenerate pressure is basically independent of T, so that the energy released by fusion does not increase the pressure and therefore leads to negligible expansion and negligible work done. All nuclear energy released therefore goes into raising the internal energy. Since the internal energy of the degenerate *electrons* is a function of ρ and hence remains almost unchanged, it is the internal energy of the non-degenerate *ions* that increases and thus raises the temperature. As a result, the evolution is vertically upward in the ρ_c-T_c diagram.[3]

The thermonuclear runaway leads to an enormous overproduction of energy: at maximum, the local luminosity in the helium core is $l \approx 10^{10}\,L_\odot$ – similar to a small galaxy! However, this only lasts for a few seconds. Since the temperature increases at almost constant density, degeneracy is eventually lifted when $T \approx 3 \times 10^8$ K. Further energy release increases the pressure when the gas starts behaving like an ideal gas and thus causes expansion and cooling. All the energy released by the thermonuclear runaway is absorbed in the expansion of the core, and none of this nuclear power reaches the surface. The expansion and cooling results in a decrease of the energy generation rate, until it balances the energy loss rate and the core settles in thermal equilibrium at $T_c \approx 10^8$ K and $\rho_c \approx 2 \times 10^4$ g/cm^3 (see Fig. 10.1). Further nuclear burning of helium is thermally stable.

Detailed numerical calculations of the helium flash indicate that this sequence of events indeed takes place, but helium is not ignited in the centre but in a spherical shell at $m \approx 0.1\,M_\odot$ where T has a maximum. This off-centre temperature maximum is due to *neutrino losses* during the preceding red giant phase. These neutrinos are not released by nuclear reactions, but by spontaneous weak interaction processes occurring at high density and temperature (see Section 6.5). Since neutrinos thus created escape without interacting with the stellar gas, this energy loss leads to effective cooling

[3]This part of the evolution is skipped in the 1 $M_\odot$ model shown in Fig. 10.1, which is why a gap appears in the evolution track. The evolution during the He flash is shown schematically as a dashed line for the 1 $M_\odot$ model in Fig. 8.4.

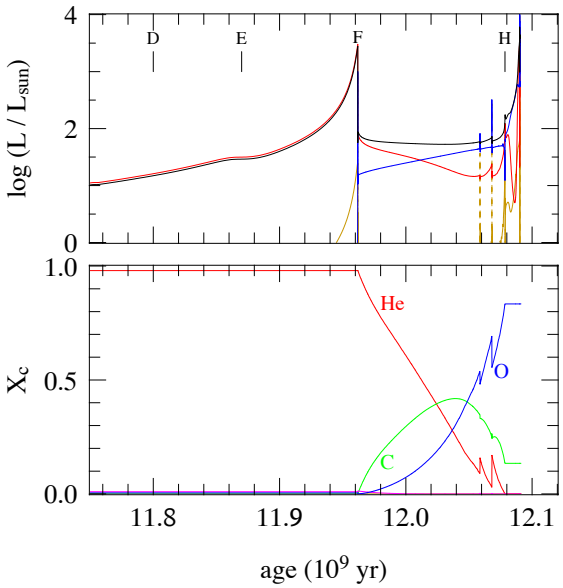

Figure 10.8. Evolution with time of the luminosities and central abundances in a $1\,M_\odot$ star during the late part of the red giant branch and during helium burning. Letters D…H correspond to the same evolution phases as in Fig. 10.5.

of the central region of the degenerate helium core. The mass coordinate at which $T_{\max}$ occurs (and where helium ignites) decreases somewhat with stellar mass.

The high local luminosity causes almost the entire region between the ignition point (at $m \approx 0.1\,M_\odot$) up to the bottom of the H-burning shell (at $0.45\,M_\odot$) to become convective. The energy released in the He flash is thus transported efficiently to the edge of the core, where it is absorbed by expansion of the surrounding non-degenerate layers. Convection also mixes the product of the He flash (^{12}C produced in the 3α reaction) throughout the core. About 3 % of the helium in the core is converted into carbon during the flash. Because the convective shell containing this carbon never overlaps with the convective envelope surrounding the H-burning shell, this carbon does not reach the surface. (However, this may be different at very low metallicity.)

After the He flash, the whole core expands somewhat but remains partially degenerate. In detailed models a series of smaller flashes follows the main He flash (see Fig. 10.7) during ≈ 1.5 Myr, before degeneracy in the centre is completely lifted and further He burning proceeds stably in a convective core, as for intermediate-mass stars.

The horizontal branch

In our $1\,M_\odot$ example star, the helium flash occurs at point F in Fig. 10.5. Evolution through the helium flash was not calculated for the model shown in this figure. Instead, the evolution of the star is resumed at point G when the helium core has become non-degenerate and has settled into TE with stable He burning in the centre and H-shell burning around the core. (Models constructed in this way turn out to be very similar to models that are computed all the way through the He flash, such as shown in Fig. 10.7.) At this stage the luminosity and radius of the star have decreased by more than an order of magnitude from the situation just before the He flash. Here we again see the mirror principle at work: in this case the core has expanded (from a degenerate to a non-degenerate state) and the envelope has simultaneously contracted, with the H-burning shell acting as a ‘mirror’.

In the $1\,M_\odot$ star of solar composition shown in Fig. 10.5, helium burning occurs between G and H. The position of the star in the H-R diagram does not change very much during this period, always staying close (but somewhat to the left of) the red giant branch. The luminosity is $\approx 50\,L_\odot$ for most

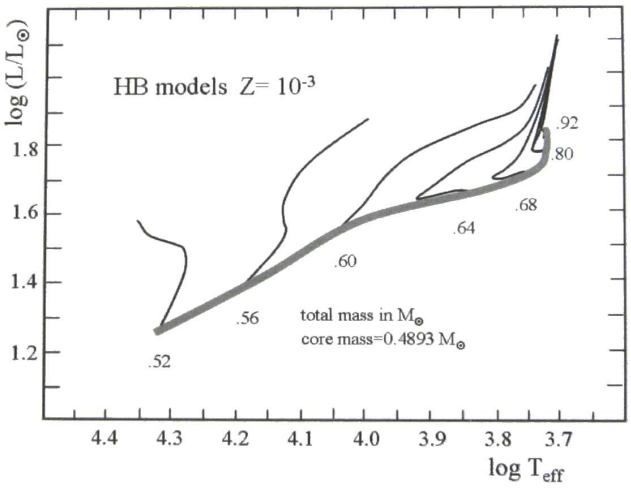

Figure 10.9. Location of the zero-age horizontal branch (think gray line) for a metallicity $Z = 0.001$ typical of globular clusters. These models have the same core mass ($0.489\,M_\odot$) but varying total (i.e. envelope) mass, which determines their position in the H-R diagram. Evolution tracks during the HB for several total mass values are shown as thin solid lines. Figure from MAEDER.

of the time; this value is determined mainly by the core mass. Since the core mass at the start of helium burning is $\approx 0.45\,M_\odot$ for all low-mass stars, independent of stellar mass, the luminosity at which He burning occurs is also almost independent of mass. If we consider He-burning stars of a given composition (e.g. in a star cluster), only the envelope mass may vary from star to star. At solar metallicity, all such stars occupy about the same position in the HRD. This gives rise to a so-called *red clump* in observed colour-magnitude diagrams of low-mass stellar populations (visible for instance in Fig. 1.1). However, the radius and effective temperature of He-burning stars depends on their envelope mass. Stars with a small envelope mass (either because of a smaller initial mass, or because they suffered a larger amount of mass loss on the RGB) can be substantially hotter than the one shown in Fig. 10.5. Furthermore, at low metallicity the critical envelope mass, below which He-burning stars become small and hot, is larger. Stars with different amounts of mass remaining in their envelopes can then form a *horizontal branch* in the HRD (Fig. 10.9). Horizontal branches are found in old stellar populations, especially in globular clusters of low metallicity (an example is the globular cluster M3 shown in Fig. 1.2). The observed distribution of stars along the HB varies greatly from cluster to cluster, and the origin of these different *HB morphologies* is not fully understood.

The duration of the core helium burning phase is about 120 Myr, again independent of stellar mass. While this is longer than in intermediate-mass stars, it is a much shorter fraction of the main-sequence lifetime because of the much higher luminosity of the He-burning phase. The evolution of the stellar structure during helium burning is qualitatively similar to that of intermediate-mass stars; see Figs. 10.5a and 10.8. The most striking differences are:

- The contribution of He-burning to the stellar luminosity is larger, especially towards the end of the phase. This is due to the relatively small envelope mass.
- The development of a substantial *semi-convective* region on top of the convective core. This is related to a difference in opacity between the C-rich convective core and the He-rich zone surrounding it, and gives rise to partial (non-homogeneous) mixing in this region.
- The occurrence of 'breathing pulses', giving rise to the sudden jumps in the central composition and in the luminosity. Whether these are real or simply a numerical artifact of one-dimensional stellar models is not clear.[4]

[4]For details about the latter two effects, see either SALARIS & CASSISI or John Lattanzio's tutorial at `http://www.maths.monash.edu.au/johnl/StellarEvolnDemo/`.

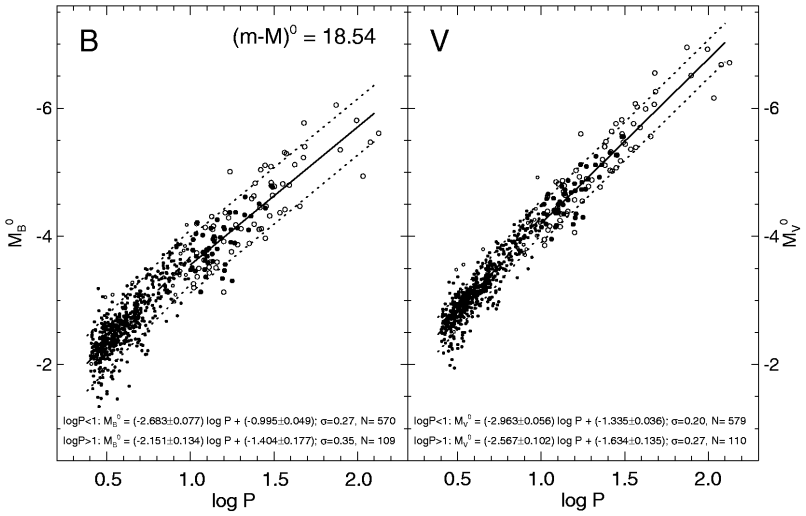

Figure 10.10. The period-luminosity relation for classical Cepheids in the Large Magellanic Cloud. Luminosity is expressed as absolute magnitude in the B band (left) and in the V band. Figure from Sandage et al. (2004, A&A 424, 43).

10.4 Pulsational instability during helium burning

During their post-main sequence evolution, stars may undergo one or more episodes during which they are unstable to radial pulsations. The most important manifestation of these pulsations are the *Cepheid* variables, luminous pulsating stars with periods between about 2 and 100 days. It turns out that there is a well-defined correlation between the pulsation period and the luminosity of these stars, first discovered for Cepheids in the Small Magellanic Cloud. A modern version of this empirical relation is shown in Fig. 10.10. Their importance for astronomy lies in the fact that the period can be easily determined, even for stars in other galaxies, and thus provides an estimate of the absolute luminosity of such a star, making Cepheids important *standard candles* for the extragalactic distance scale.

Cepheids lie along a pulsational instability strip in the H-R diagram (see Fig. 10.11). During the evolution of an intermediate-mass star, this instability strip is crossed up to three times. The first crossing occurs during H-shell burning (C–D in Fig. 10.2) but this is such a rapid phase that the probability of catching a star in this phase is very small. In stars with sufficiently extended blue loops, another two crossings occur (F-G and G–H) during a much slower evolution phase. Cepheids must thus be helium-burning stars undergoing a blue loop. Equivalently, the *RR Lyrae* variables seen in old stellar populations lie along the intersection of the instability strip and the horizontal branch.

Since pulsation is a dynamical phenomenon, the pulsation period is closely related to the dynamical timescale (eq. 2.18). Therefore the pulsation period Π is related the mean density: to first approximation once can write $\Pi \propto \bar{\rho}^{-1/2} \propto M^{-1/2}R^{3/2}$. Each passage of the instability strip yields a fairly well-defined radius and luminosity. Passage at a larger L corresponds to a larger R and therefore to a larger Π, because the variation in mass is smaller than that in radius and enters the relation with a smaller power. This provides a qualitative explanation of the period-luminosity relation. The minimum observed period should correspond to the the lowest-mass star undergoing a blue loop. Also the number of Cepheids as a function of period must correspond to the time it takes for a star of the corresponding mass to cross the instability strip. Thus Cepheids provide a potential test of stellar evolution models.

10.4.1 Physics of radial stellar pulsations

The radial oscillations of a pulsating star result from pressure waves, i.e sound waves that resonate in the stellar interior. These radial oscillation modes are essentially standing waves, with a node at the centre and an open end at the stellar surface – not unlike the sound waves in an organ pipe. Similarly, there are several possible modes of radial pulsation, the *fundamental mode* having just one node at the centre, while the *first* and *second overtone* modes have one or two additional nodes between the centre and surface, etc. Most radially pulsating stars, such as Cepheids, are oscillating in their fundamental mode.

In order to understand what powers the pulsations of stars in the instability strip, let us first reconsider the dynamical stability of stars. We have seen in Sec. 7.5.1 that overall dynamical stability requires $\gamma_{\rm ad} > \frac{4}{3}$. In this situation a perturbation of pressure equilibrium will be restored, the restoring force being larger the more $\gamma_{\rm ad}$ exceeds the critical value of $\frac{4}{3}$. In practice, due to the inertia of the layers under consideration, this will give rise to an *oscillation* around the equilibrium structure. A linear perturbation analysis of the equation of motion (2.11) shows that a layer at mass coordinate m having equilibrium radius r_0 will undergo radial oscillations with a frequency

$$\omega^2 = (3\gamma_{\rm ad} - 4)\,\frac{Gm}{r_0^3}, \tag{10.4}$$

if we assume the oscillations are adiabatic. Note that $\omega^2 > 0$ as long as $\gamma_{\rm ad} > \frac{4}{3}$, consistent with dynamical stability. On the other hand, for $\gamma_{\rm ad} < \frac{4}{3}$ the frequency becomes imaginary, which indicates

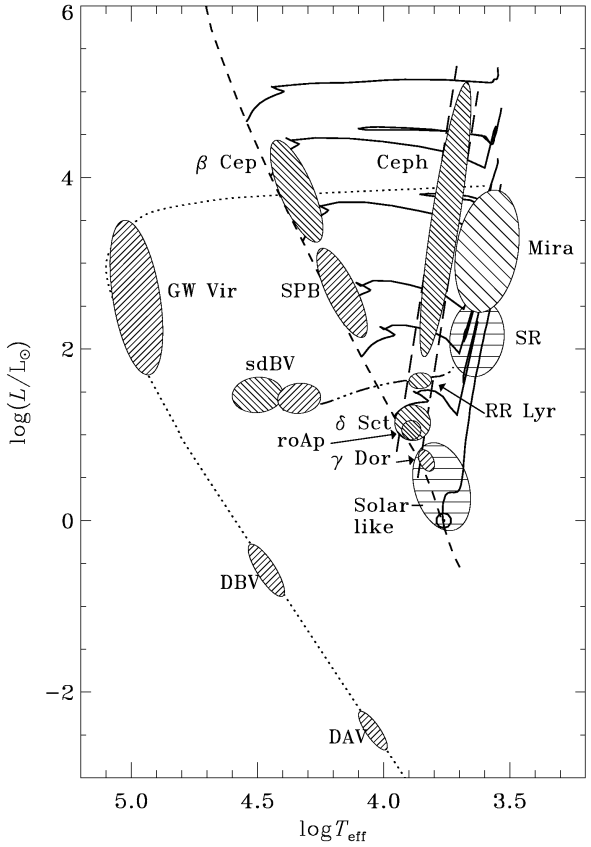

Figure 10.11. Occurrence of various classes of pulsating stars in the H-R diagram, overlaid on stellar evolution tracks (solid lines). Cepheid variables are indicated with 'Ceph', they lie within the pulsational instability strip in the HRD (long-dashed lines). Their equivalents are the RR Lyrae variables among HB stars (the horizontal branch is shown as a dash-dotted line), and the δ Scuti stars (δ Sct) among main-sequence stars. Pulsational instability is also found among luminous red giants (Mira variables), among massive main-sequence stars – β Cep variables and slowly pulsating B (SPB) stars, among extreme HB stars known as subdwarf B stars (sdBV) and among white dwarfs. Figure from Christensen-Dalsgaard (2004).

an exponential growth of the perturbation, i.e. dynamical instability. A proper average of ω over the star yields the pulsation frequency of the fundamental mode. We can obtain an approximate expression by replacing m with the total mass M and r_0 by the radius R, and taking $\gamma_{\rm ad}$ constant throughout the star. This yields

$$\Pi_0 = \frac{2\pi}{\sqrt{(3\gamma_{\rm ad}-4)\,GM/R^3}} = \left(\frac{3\pi}{(3\gamma_{\rm ad}-4)\,G\bar{\rho}}\right)^{1/2}. \tag{10.5}$$

This is indeed the same expression as for the dynamical timescale, to within a factor of unity. One can write

$$\Pi = Q\left(\frac{\bar{\rho}}{\bar{\rho}_\odot}\right)^{-1/2}, \tag{10.6}$$

where the pulsation constant Q depends on the structure of the star and is different for different modes of pulsation. For the fundamental mode, $Q \approx 0.04$ days and Q is smaller for higher overtones.

Driving and damping of pulsations

In an exactly adiabatic situation the oscillations will maintain the same (small) amplitude. In reality the situation is never exactly adiabatic, which means that the oscillations will generally be damped, unless there is an instability that drives the oscillation, i.e. that makes their amplitude grow.

The requirement for growth of an oscillation is that the net work done by a mass element in the star on its surroundings during an oscillation cycle must be positive, $\oint P\,{\rm d}V > 0$. By the first law of thermodynamics, this work is provided by a net amount of heat being absorbed by the element during the cycle,

$$\oint {\rm d}Q = \oint P\,{\rm d}V > 0.$$

The change in entropy of the mass element is ${\rm d}S = {\rm d}Q/T$. Since entropy is a state variable, $\oint {\rm d}Q/T = 0$ during a pulsation cycle. A mass element maintaining constant T during a cycle therefore cannot absorb any heat. Suppose that the temperature undergoes a small variation $T(t) = T_0 + \delta T(t)$ around an average value T_0. Then

$$0 = \oint \frac{{\rm d}Q}{T} = \oint \frac{{\rm d}Q}{T_0+\delta T} \approx \oint \frac{{\rm d}Q}{T_0}\left(1-\frac{\delta T}{T_0}\right), \tag{10.7}$$

or

$$\oint {\rm d}Q \approx \oint {\rm d}Q\,\frac{\delta T}{T_0}. \tag{10.8}$$

Eq. (10.8) means that heat must enter the element (${\rm d}Q > 0$) when the temperature is high ($\delta T > 0$), i.e. when the layer is compressed, and/or heat must leave the layer (${\rm d}Q < 0$) during the low-temperature part of the cycle ($\delta T < 0$), i.e. during expansion. This is known in thermodynamics as a *heat engine*, and is analogous to what happens in a normal combustion motor, such as a car engine. In a pulsating star, some layers may absorb heat and do work to drive the pulsation, while other layers may lose heat and thereby damp the pulsation (if $\oint {\rm d}Q = \oint P\,{\rm d}V < 0$). To determine the overall effect, the contributions $\oint P\,{\rm d}V$ must be integrated over all mass layers in the star.

In stars there are two possible mechanisms that can drive pulsations:

- If nuclear reactions occur in a region that is compressed during a pulsation, then the increase in T will lead to an increase in the energy generation rate $\epsilon_{\rm nuc}$. This satisfies the criterion (10.8) and is known as the *ϵ-mechanism*. Although this is always present, the amplitudes of the oscillations induced by this mechanism in the core of a star are usually so small that it cannot drive any significant pulsations. It may have important effects in very massive stars, but it is certainly not relevant for explaining Cepheid pulsations.

- If during the compression of a layer it becomes more *opaque*, then the energy flowing through this layer will be 'trapped'. The resulting increase in temperature and pressure pushes the layer outward. During the resulting expansion, the gas will become more transparent again and release the trapped heat. This so-called *κ-mechanism* can thus maintain the oscillation cycle and drive radial pulsations.

The condition for the κ-mechanism to work is therefore that the opacity must increase when the gas is compressed. The compression during a pulsation cycle is not exactly adiabatic, otherwise the mechanism would not work, but it is very close to adiabatic. Then the condition can be written as $(\mathrm{d}\ln\kappa/\mathrm{d}\ln P)_{\rm ad} > 0$. We can write this as

$$\left(\frac{\mathrm{d}\ln\kappa}{\mathrm{d}\ln P}\right)_{\rm ad} = \left(\frac{\partial\ln\kappa}{\partial\ln P}\right)_T + \left(\frac{\partial\ln\kappa}{\partial\ln T}\right)_P \left(\frac{\mathrm{d}\ln T}{\mathrm{d}\ln P}\right)_{\rm ad} \equiv \kappa_P + \kappa_T\,\nabla_{\rm ad}, \tag{10.9}$$

where κ_P and κ_T are shorthand notation for the partial derivatives of $\ln\kappa$ with respect to $\ln P$ and $\ln T$, respectively. For successful pulsations we must therefore have

$$\kappa_P + \kappa_T\,\nabla_{\rm ad} > 0. \tag{10.10}$$

The instability strip and the period-luminosity relation

In stellar envelopes the opacity can be roughly described by a Kramers law, $\kappa \propto \rho T^{-3.5}$, which when combined with the ideal-gas law implies $\kappa_P \approx 1$ and $\kappa_T \approx -4.5$. Since for an ionized ideal gas $\nabla_{\rm ad} = 0.4$, we normally have $\kappa_P + \kappa_T\,\nabla_{\rm ad} < 0$, i.e. κ decreases upon compression and the star will not pulsate. In order to satisfy (10.10) one must have either:

- $\kappa_T > 0$, which is the case when the H^- opacity dominates, at $T < 10^4\,\mathrm{K}$. This may contribute to the driving of pulsations in very cool stars, such as Mira variables (Fig. 10.11), but the Cepheid instability strip is located at too high $T_{\rm eff}$ for this to be important.

- In case of a Kramers-like opacity, a small value of $\nabla_{\rm ad}$ can lead to pulsation instability. For $\kappa_P \approx 1$ and $\kappa_T \approx -4.5$, eq. (10.10) implies $\nabla_{\rm ad} \lesssim 0.22$. Such small values of $\nabla_{\rm ad}$ can be found in *partial ionization zones*, as we have seen in Sec. 3.5 (e.g. see Fig. 3.5).

Stars generally have two important partial ionization zones, one at $T \approx 1.5\times10^4\,\mathrm{K}$ where both $\mathrm{H} \leftrightarrow \mathrm{H}^+ + \mathrm{e}^-$ and $\mathrm{He} \leftrightarrow \mathrm{He}^+ + \mathrm{e}^-$ occur, and one at $T \approx 4\times10^4\,\mathrm{K}$ where helium becomes twice ionized ($\mathrm{He}^+ \leftrightarrow \mathrm{He}^{++} + \mathrm{e}^-$). These partial ionization zones can explain the location of the instability strip in the H-R diagram, as follows.

- At large $T_{\rm eff}$ (for $T_{\rm eff} \gtrsim 7500\,\mathrm{K}$, the 'blue edge' of the instability strip) both ionization zones lie near the surface, where the density is very low. Although this region is indeed non-adiabatic, the mass and heat capacity of these zones is too small to drive pulsations effectively.

- As $T_{\rm eff}$ decreases, the ionization zones lie deeper into the stellar envelope. The mass and heat capacity in the partial ionization zones increase, while remaining non-adiabatic enough to absorb sufficient heat to drive pulsations.

- At still smaller $T_{\rm eff}$ (for $T_{\rm eff} \lesssim 5500\,{\rm K}$, the 'red edge' of the instability strip) the partial ionization zones lie at such high density that the gas behaves almost adiabatically. Although these zones still have a destabilizing effect, they cannot absorb enough heat to make the star as a whole unstable.

Thus the instability strip occupies a narrow region in the H-R diagram, as indicated in Fig. 10.11. Its location is related to the depth of the partial ionization zones. Since these zones occur in a specific temperature range, the instability strip also occurs for a narrow range of $T_{\rm eff}$ values, and is almost vertical in the H-R diagram (and parallel to the Hayashi line).

We can understand the period-luminosity relation from the dependence of the pulsation period on mass and radius (eq. 10.6). Since Cepheids follow a mass-luminosity relation, $M \propto L^{\alpha}$, and since $L \propto R^2 T_{\rm eff}^4$, we can write

$$\Pi \propto Q\,\frac{R^{3/2}}{M^{1/2}} \propto Q\,\frac{L^{(3/4)-(1/2\alpha)}}{T_{\rm eff}^3}.$$

With $\alpha \approx 3$ and $T_{\rm eff} \approx$ constant, we find $\Pi \propto L^{0.6}$ or $\log L \approx 1.7\,\log\Pi$ + const. Detailed numerical models give

$$\log L = 1.270\,\log\Pi + 2.570 \tag{10.11}$$

for the blue edge, and a slope of 1.244 and a constant 2.326 for the red edge. The smaller slope than in the simple estimate is mainly due to the fact that the effective temperature of the instability strip is not constant, but slightly decreases with increasing L.

Suggestions for further reading

The contents of this chapter are also covered by Chapters 25.3.2 and 26.1–26.5 of Maeder, while stellar pulsations and Cepheids are treated in detail in Chapter 15. See also Kippenhahn & Weigert, Chapters 31 and 32.

Exercises

10.1 Conceptual questions

(a) Why does the luminosity of a star increase on the main sequence? Why do low-mass stars, like the Sun, expand less during the main sequence than higher-mass stars?

(b) Explain what happens during the 'hook' at the end of the main sequence of stars more massive than the Sun.

(c) What is *convective overshooting*? Think of at least three effects of overshooting on the evolution of a star.

(d) Explain the existence of a *Hertzsprung gap* in the HRD for high-mass stars. Why is there no Hertzsprung gap for low-mass stars?

(e) What do we mean by the *mirror principle*?

(f) Why does the envelope become convective on the red giant branch? What is the link with the *Hayashi line*?

10.2 Evolution of the abundance profiles

(a) Use Fig. 10.3 to sketch the profiles of the hydrogen and helium abundances as a function of the mass coordinate in a $5\,M_\odot$ star, at the ages corresponding to points C, E, G and H. Try to be as quantitative as possible, using the information provided in the figure.

(b) Do the same for a $1\,M_\odot$ star, using Figs. 10.5 and 10.8, at points B, D, F and H.

(c) The abundances plotted in Figs. 10.3 and 10.8 are central abundances. What happens to the abundances at the surface?

10.3 Red giant branch stars

(a) Calculate the total energy of the Sun assuming that the density is constant, i.e. using the equation for potential energy $E_{\rm gr} = -\frac{3}{5}GM^2/R$. In later phases, stars like the Sun become red giants, with $R \approx 100R_\odot$. What would be the total energy, if the giant had constant density. Assume that the mass did not change either. Is there something wrong? If so, why is it?

(b) What really happens is that red giants have a dense, degenerate, pure helium cores which grow to $\sim 0.45M_\odot$ at the end of the red giant branch (RGB). What is the maximum radius the core can have for the total energy to be smaller than the energy of the Sun? (N.B. Ignore the envelope – why are you allowed to do this?)

(c) For completely degenerate stars, one has

$$R = 2.6 \times 10^9\, {\mu_e}^{-5/3} \left(\frac{M}{M_\odot}\right)^{-1/3} \text{cm}, \tag{10.12}$$

where μ_e is the molecular weight per electron and $\mu_e = 2$ for pure helium. Is the radius one finds from this equation consistent with upper limit derived in (b)?

10.4 Core mass-luminosity relation for RGB stars

Low-mass stars on the RGB obey a core mass-luminosity relation, which is approximately given by eq. (10.2). The luminosity is provided by hydrogen shell burning.

(a) Derive relation between luminosity L and the rate at which the core grows $\mathrm{d}M_{\rm c}/\mathrm{d}t$. Use the energy released per gram in hydrogen shell burning.

(b) Derive how the core mass evolves in time, i.e, $M_{\rm c} = M_{\rm c}(t)$.

(c) Assume that a star arrives to the RGB when its core mass is 15% of the total mass, and that it leaves the RGB when the core mass is $0.45\,M_\odot$. Calculate the total time a $1\,M_\odot$ star spends on the RGB and do the same for a $2\,M_\odot$ star. Compare these to the main sequence (MS) lifetimes of these stars.

(d) What happens when the core mass reaches $0.45\,M_\odot$? Describe the following evolution of the star (both its interior and the corresponding evolution in the HRD).

(e) What is the difference in evolution with stars more massive than $2\,M_\odot$?

10.5 Jump in composition

Consider a star with the following distribution of hydrogen:

$$X(m) = \begin{cases} 0.1 & \text{for } m < m_c \\ 0.7 & \text{for } m \le m_c \end{cases} \tag{10.13}$$

(a) In this star a discontinuous jump in the composition profile occurs at $m = m_c$. What could have caused such a chemical profile? Explain why P and T must be continuous functions.

(b) Calculate the jump in density $\Delta\rho/\rho$.

(c) Also calculate the jump in opacity, $\Delta\kappa/\kappa$, if the opacity is given as:
- Kramers: $\kappa_{bf} \sim Z(1+X)\rho T^{-3.5}$
- Electron scattering: $\kappa_e = 0.2(1+X)$